Control of exciton-photon interactions in CuCl microcavities

M. Nakayama,[*] K. Miyazaki, T. Kawase, and D. Kim

Department of Applied Physics, Graduate School of Engineering, Osaka City University, 3-3-138 Sugimoto,
Sumiyoshi-ku, Osaka 558-8585, Japan

We have investigated the active-layer-thickness dependence of exciton-photon interactions in planar CuCl microcavities with HfO_2/SiO_2 distributed Bragg reflectors. The active layer thickness was changed from $\lambda/32$ to $\lambda/4$, while the cavity length was fixed at $\lambda/2$. We performed angle-resolved reflectance measurements and clearly detected three cavity-polariton modes, originating from the lower, middle, and upper polariton branches, in a strong-coupling regime of the Z_3 and $Z_{1,2}$ excitons and cavity photon. The incidence-angle dependence of the cavity-polariton modes was analyzed using a phenomenological Hamiltonian for the strong coupling. It was found that the interaction energies of the cavity-polariton modes, the so-called vacuum Rabi splitting energies, are systematically controlled from 22(37) to 71(124) meV for the $Z_3(Z_{1,2})$ exciton by changing the active layer thickness from $\lambda/32$ to $\lambda/4$. The active-layer-thickness dependence of the Rabi splitting energy is quantitatively explained by a simple theory for quantum-well microcavities.

PACS number(s): 78.67.Pt, 71.36.+c, 71.35.−y

I. INTRODUCTION

Exciton polaritons in semiconductor microcavities, so-called cavity polaritons, are admixed quasiparticles resulting from the strong coupling between excitons and cavity photons.[1] The cavity polariton has attracted much attention from the aspects of Bose-Einstein condensation,[2–5] polariton lasing,[6–8] and high-efficiency generation of entangled photons.[9,10] The interaction energy between the exciton and the cavity photon, the so-called vacuum Rabi splitting energy, is one of the key factors determining the characteristics of the cavity polariton. The Rabi splitting energy mainly depends on the oscillator strength of the exciton and the overlap between the exciton and the photon-field wave functions.[11] In GaAs and GaN bulk microcavities, the Rabi splitting energies are around 5 and 40 meV,[11,12] respectively. A giant Rabi splitting energy that is ∼100 meV was realized in a CuCl bulk microcavity.[13] It is well known that the splitting energy (Δ_{LT}) between the longitudinal and the transverse excitons is a measure of the excitonic oscillator strength. The values of Δ_{LT} are 0.08,[14] 1.0,[15] and 5.7 meV[16] for GaAs, GaN, and CuCl, respectively. The reported Rabi splitting energies are arranged in order of Δ_{LT}. From the viewpoint of entangled photon generation utilizing biexciton-resonant hyperparametric scattering (BRHS) in microcavities,[10] which is desired in quantum infocommunication technology, the control of the Rabi splitting energy is essential to achieve the phase-matching condition in the BRHS process. CuCl is quite advantageous for the BRHS because the biexciton binding energy is very high: 34 meV.[16] Thus, the systematic control of the Rabi splitting energies in CuCl microcavities is significant in future applications of the high-efficiency generation of entangled photons. One of the principles for controlling the Rabi splitting energy is to change the active-layer-thickness, resulting in varying the overlap between the exciton and the photon-field wave functions. Note that little has been known about the experimental demonstration of systematic control of the Rabi splitting energies in microcavities.

In the present work, we have controlled the Rabi splitting energies in CuCl microcavities with HfO_2/SiO_2 distributed Bragg reflectors (DBRs) by changing the active-layer thickness from $\lambda/32$ to $\lambda/4$, where λ corresponds to an effective resonant wavelength of the lowest-lying Z_3 exciton. CuCl has two exciton states, called Z_3 and $Z_{1,2}$. The Z_3 ($Z_{1,2}$) exciton is assigned to the split-off-hole exciton(degenerate heavy-hole and light-hole excitons). From angle-resolved reflectance measurements, we clearly detect three cavity-polariton modes originating from the lower, middle, and upper polariton branches (LPB, MPB, and UPB) in a strong coupling regime of the Z_3 and $Z_{1,2}$ excitons, and cavity photon. The Rabi splitting energies are estimated by analyzing the cavity-polariton dispersions with a phenomenological 3×3 Hamiltonian for the strong coupling. The active-layer-thickness dependence of the Rabi splitting energy is quantitatively discussed with a simple theory for quantum-well (QW) microcavities.

II. EXPERIMENTS

We prepared CuCl microcavities with HfO_2/SiO_2 DBRs on a (0001) Al_2O_3 substrate. The cavity was sandwiched by the DBRs. The bottom and top DBRs consisted of 9.5 and 8.5 periods, respectively, and each DBR was terminated by the HfO_2 layer. The HfO_2 and SiO_2 layers were fabricated at room temperature by radio-frequency (rf) magnetron sputtering. Commercially supplied plates of HfO_2 with a purity of 3N and SiO_2 with a purity of 4N were used as the targets. The sputtering gas was Ar under a pressure of ∼1.0 Pa. The cavity consisted of a CuCl active layer and SiO_2 spacer layers. The CuCl active layer, which was grown at 60°C by vacuum deposition using CuCl powders with a purity of 4N in 7×10^{-6} Pa, was set at the central position of the cavity. The cavity length was fixed at $\lambda/2$, while the active layer thickness was changed from $\lambda/32$ to $\lambda/4$. The effective length λ is given by $\lambda_{Z(3)}/n_b$, where $\lambda_{Z(3)}$ is the resonant wavelength of the Z_3 exciton in vacuum, and n_b is the background refractive index. The values of n_b for CuCl, HfO_2, and SiO_2 are 2.36,[16] 2.05,[17] and 1.50,[17] respectively. The thicknesses of the HfO_2 and SiO_2 layers in the DBR were designed as $\lambda/4$. The growth rates of the CuCl, HfO_2, and SiO_2 layers were precisely monitored during the deposition process

using a crystal oscillator. We confirmed from x-ray diffraction patterns that the crystalline CuCl layer is just oriented along the [111] axis. The quality factor of the microcavity was estimated to be ∼250 from an empty cavity. Although CuCl is a hygroscopic material, we already demonstrated that the CuCl microcavity with the HfO_2/SiO_2 DBRs is robust.[18] In measurements of angle-resolved reflectance spectra, the probe light source was a Xe lamp, and the reflected light was detected with a charge-coupled device attached to a 32-cm single monochromator with a resolution of 0.15 nm. We did not perform polarization analysis of reflected light.

III. RESULTS AND DISCUSSION

Angle-resolved reflectance spectra at 10 K in the CuCl microcavity with an active layer thickness of $\lambda/4$ (designed thickness, 41 nm) are shown in Fig. 1(a). We clearly observe three dip structures in each reflectance spectrum. As described above, in the CuCl microcavity, there are three cavity-polariton branches because of the strong coupling between the Z_3 and $Z_{1,2}$ excitons and cavity photon; therefore, the three dip structures are assigned to the LPB, MPB, and UPB, respectively, in order of energy. Dashed curves are the guides for the eye. The incidence-angle dependence of the LPB, MPB, and UPB modes exhibits the profiles of the cavity-polariton dispersions.

To analyze the experimental results of the incidence-angle dependence, the eigenenergies of the cavity polaritons are calculated using a phenomenological Hamiltonian given by the matrix[13]

$$\begin{pmatrix} E_{\mathrm{cav}}(\theta) & \Omega_3/2 & \Omega_{1,2}/2 \\ \Omega_3/2 & E_{Z(3)} & 0 \\ \Omega_{1,2}/2 & 0 & E_{Z(1,2)} \end{pmatrix}, \quad (1)$$

where $E_{Z(3)}$ and $E_{Z(1,2)}$ are the energies of the Z_3 and $Z_{1,2}$ excitons, respectively, and $\Omega_3(\Omega_{1,2})$ is the Rabi splitting energy related to the $Z_3(Z_{1,2})$ exciton. The energy of the cavity photon, $E_{\mathrm{cav}}(\theta)$, is given by[19]

$$E_{\mathrm{cav}}(\theta) = E_0 \left(1 - \frac{\sin^2 \theta}{n_{\mathrm{eff}}^2}\right)^{-1/2}, \quad (2)$$

where θ and n_{eff} are the incidence angle and the effective refractive index of the cavity, respectively, and E_0 is the energy of the cavity photon at $\theta = 0°$. Figure 1(b) shows the experimental results of the incidence-angle dependence of the LPB, MPB, and UPB energies (filled circles) and the cavity-polariton dispersions fitted to the data using Eq. (1) (solid curves), where the horizontal dashed lines indicate the energies of the Z_3 and $Z_{1,2}$ excitons, and the dashed curve depicts the dispersion of the cavity photon. The energies of the Z_3 and $Z_{1,2}$ excitons were obtained from the absorption spectrum of a CuCl film: 3.204 eV for Z_3 and 3.273 eV for $Z_{1,2}$. The fitting parameters are $\Omega_{1,2}$, Ω_3, E_0, and n_{eff}, where the adjusted value of n_{eff} is 1.72 in this case. It is obvious that the experimental results are well explained by Eq. (1). The Rabi splitting energies of Ω_3 and $\Omega_{1,2}$ are evaluated as 71 and 124 meV, respectively, where the error in the evaluation is $\pm 5\%$. Since the $Z_{1,2}$ exciton is the degenerate heavy-hole and light-hole excitons, its oscillator strength is higher than that of
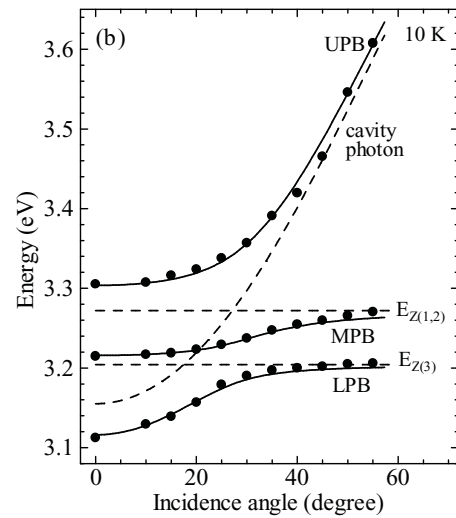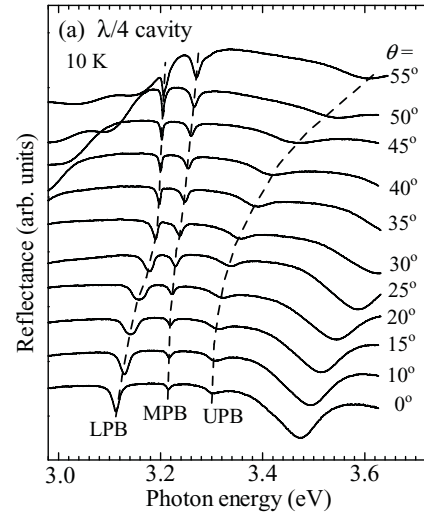

FIG. 1. (a) Angle-resolved reflectance spectra at 10 K in a CuCl microcavity with an active layer thickness of $\lambda/4$, where dashed curves are guides for the eye. (b) Experimental results on the incidence-angle dependence of the LPB, MPB, and UPB energies (filled circles) and the cavity-polariton dispersions fitted to the data using Eq. (1) (solid curves), where the horizontal dashed lines indicate the energies of the Z_3 and $Z_{1,2}$ excitons, and the dashed curve depicts the dispersion of the cavity photon.

the Z_3 exciton. The value of $\Omega_{1,2}$, therefore, is larger than that of Ω_3.

Figure 2(a) shows the angle-resolved reflectance spectra at 10 K in a CuCl microcavity with an active layer thickness of $\lambda/32$ (designed thickness, 5 nm). Experimental results on the incidence-angle dependence of the LPB, MPB, and UPB energies (filled circles) and the cavity-polariton dispersions fitted to the data using Eq. (1) (solid curves) are depicted in Fig. 2(b). The Rabi splitting energies of Ω_3 and $\Omega_{1,2}$ are evaluated as 22 and 37 meV, respectively. It is evident that the Rabi splitting energies markedly decrease with a decrease in the active layer thickness from $\lambda/4$ to $\lambda/32$.

The active-layer-thickness dependence of the Rabi splitting energies (Ω_3 and $\Omega_{1,2}$) estimated from the incidence-angle dependence of the LPB, MPB, and UPB energies using Eq.(1) is shown in Fig. 3, where the filled and open circles
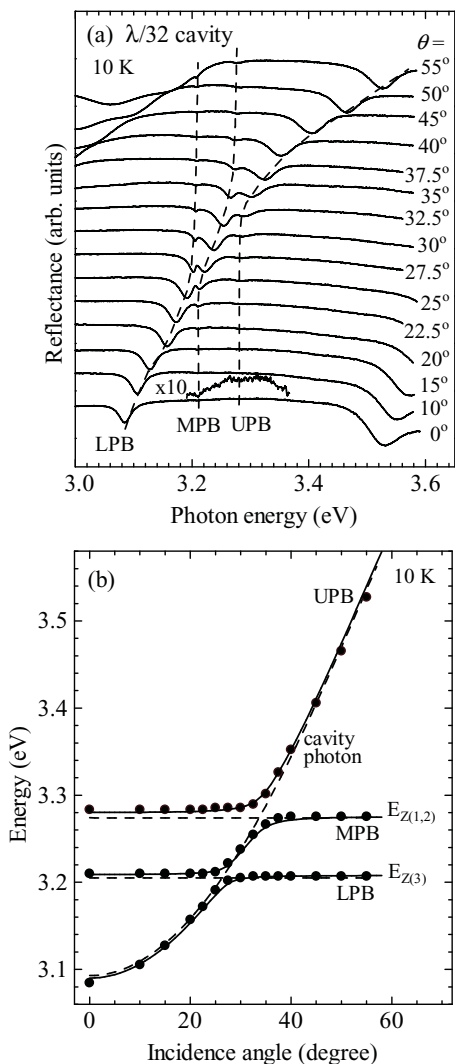
FIG. 2. (a) Angle-resolved reflectance spectra at 10 K in a CuCl microcavity with an active-layer thickness of $\lambda/32$, where dashed curves are guides for the eye. (b) Experimental results on the incidence-angle dependence of the LPB, MPB, and UPB energies (filled circles) and the cavity-polariton dispersions fitted to the data using Eq. (1) (solid curves), where the horizontal dashed lines indicate the energies of the Z_3 and $Z_{1,2}$ excitons, and the dashed curve depicts the dispersion of the cavity photon.

indicate Ω_3 and $\Omega_{1,2}$, respectively. The Rabi splitting energies systematically increase with an increase in the active-layer thickness. Since the active-layer thicknesses are sufficiently smaller than $\lambda/2$, we adopt a simple model to analyze the active-layer-thickness dependence of Rabi splitting energies for QW microcavities. According to Refs. [11] and [20], the Rabi splitting energy is given by the following equation:

$$\Omega = 2\sqrt{\frac{E_{EX}\Delta_{LT}d}{L_C + L_{DBR}}}, \qquad (3)$$

where E_{EX}, d, and L_C are the exciton energy, active-layer thickness, and cavity length, respectively. L_{DBR} represents a mirror penetration depth in the DBR.[21] For simplicity, we assume that the incidence angle is zero and that the $\lambda/4$
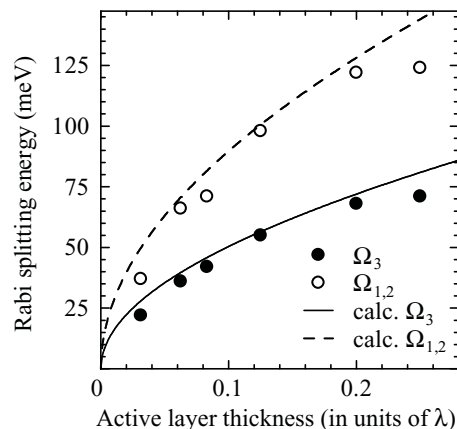

FIG. 3. Active-layer-thickness dependence of Ω_3 (filled circles) and $\Omega_{1,2}$ (open circles) estimated from the incidence-angle dependence of the LPB, MPB, and UPB energies using Eq. (1). The solid(dashed) curve indicates the active-layer-thickness dependence of $\Omega_3(\Omega_{1,2})$ calculated using Eq. (3).

condition is exactly satisfied in the DBR with a large number of periods, which leads to the following expression of L_{DBR}:

$$L_{DBR} = \frac{1}{2}\frac{\lambda_{EX}}{n_1 - n_2}, \qquad (4)$$

where λ_{EX} is the resonant wavelength of the exciton, and n_1 (n_2) corresponds to the refractive index of HfO$_2$(SiO$_2$): $L_{DBR} = 352$ nm in this case. Note that Eq. (4) holds for $n_1 > n_2$; namely, the optical wave in the cavity has a node at the cavity/DBR interface. On the basis of Eq. (3), we calculate the Rabi splitting energies of Ω_3 and $\Omega_{1,2}$ using the values of Δ_{LT}: 5.7 meV for the Z_3 exciton[16] and 18 meV for the $Z_{1,2}$ exciton.[22] The solid(dashed) curve in Fig. 3 indicates the calculated active-layer-thickness dependence of $\Omega_3(\Omega_{1,2})$. Despite the fact that there is no fitting parameter, the calculated active-layer-thickness dependence of the Rabi splitting energies well explains the experimental results. In the $\lambda/4$ microcavity, the deviation between calculated and experimental results is relatively large. This suggests that the QW approximation is not satisfactory in the $\lambda/4$ thickness.

Here, we briefly discuss a comparison of the Rabi splitting energies obtained in this work with those in other wide-gap semiconductor microcavities. Note that the thicknesses of the active layers should be the same in order to compare the Rabi splitting energies. In Ref. [23], the Rabi splitting energy is reported as 55 meV for A and B excitons in a $\lambda/4$ ZnO microcavity with Al$_{0.2}$Ga$_{0.8}$N/AlN DBRs, where the A and B excitons are not spectrally resolved because of the line-shape broadening. The Rabi splitting energy in the $\lambda/4$ CuCl microcavity is 71 meV for the Z_3 exciton as described above. It is evident from Eq. (3) that the Rabi splitting energy depends on the square root of Δ_{LT}. For the ZnO microcavity, the value of Δ_{LT} is assumed to be the average of those of the A and B excitons (2.0 and 11.1 meV):[24] 6.6 meV. Since Δ_{LT} for the Z_3 exciton of CuCl is 5.7 meV, the ratio of the Rabi splitting energy in the CuCl microcavity to that in the ZnO microcavity is expected to be 1 : 1.08, which is inconsistent with the experimental result that is 1 : 0.77. This inconsistency
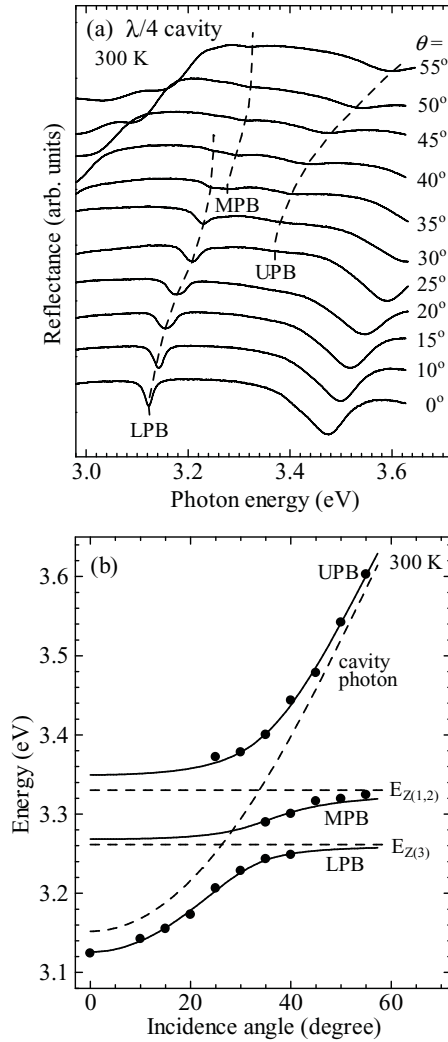
FIG. 4. (a) Angle-resolved reflectance spectra at 300 K in the CuCl microcavity with an active layer thickness of $\lambda/4$, where dashed curves are guides for the eye. (b) Experimental results on the incidence-angle dependence of the LPB, MPB, and UPB energies (filled circles) and the cavity-polariton dispersions fitted to the data using Eq. (1) (solid curves), where the horizontal dashed lines indicate the energies of the Z_3 and $Z_{1,2}$ excitons, and the dashed curve depicts the dispersion of the cavity photon.

may be due to the difference in the DBR structures connected with the values of L_{DBR} in Eq. (3).

Finally, we discuss the thermal stability of the strong coupling leading to the formation of cavity polaritons in the CuCl microcavity. Figure 4(a) shows the angle-resolved reflectance spectra in the $\lambda/4$ CuCl microcavity at 300 K. It is evident from Fig. 4(a) that the three dip structures assigned to the LPB, MPB, and UPB modes are observed, though the thermal broadening of the line shapes weakens the intensities of the three modes. The experimental results of the incidence-angle dependence of the LPB, MPB, and UPB energies (filled circles) and the cavity-polariton dispersions fitted to the data using Eq. (1) (solid curves) are depicted in Fig. 4(b). The Rabi splitting energies of Ω_3 and $\Omega_{1,2}$ are evaluated as 70 and 119 meV, respectively, which are consistent with the values at 10 K. This fact demonstrates that the strong coupling regime in the CuCl microcavity is maintained even at room temperature.

IV. CONCLUSIONS

We have clearly detected the three cavity-polariton branches (LPB, MPB, and UPB) from angle-resolved reflectance spectra in CuCl microcavities of various active layer thicknesses, from $\lambda/32$ to $\lambda/4$. Vacuum Rabi splitting energies (Ω_3 and $\Omega_{1,2}$) were estimated from an analysis of the incidence-angle dependence of the energies of the LPB, MPB, and UPB modes with the phenomenological Hamiltonian. It is demonstrated that the Rabi splitting energies are systematically controlled by changing the active-layer thickness. The active-layer-thickness dependence of Ω_3 and $\Omega_{1,2}$ is explained by a simple model for QW microcavities. Systematic control of Rabi splitting energies is promising for future applications of CuCl microcavities in high-efficiency generation of entangled photons.[10] In addition, it is confirmed that the strong-coupling regime in the CuCl microcavity is maintained even at room temperature.

*nakayama@a-phys.eng.osaka-cu.ac.jp

[1] For a review, A. V. Kavokin, J. J. Baumberg, G. Malpuech, and F. P. Laussy, *Microcavities* (Oxford University Press, Oxford, 2007).

[2] M. Richard, J. Kasprzak, R. André, R. Romestain, Le Si Dang, G. Malpuech, and A. Kavokin, Phys. Rev. B **72**, 201301(R) (2005).

[3] R. Balili, V. Hartwell, D. Snoke, L. Pfeiffer, and K. West, Science **316**, 1007 (2007).

[4] J. Kasprzak, D. D. Solnyshkov, R. André, Le Si Dang, and G. Malpuech, Phys. Rev. Lett. **101**, 146404 (2008).

[5] J. Levrat, R. Butté, E. Feltin, J.-F. Carlin, N. Grandjean, D. Solnyshkov, and G. Malpuech, Phys. Rev. B **81**, 125305 (2010).

[6] A. Imamoglu, R. J. Ram, S. Pau, and Y. Yamamoto, Phys. Rev. A **53**, 4250 (1996).

[7] S. Christopoulos, G. Baldassarri Höger von Högersthal, A. J. D. Grundy, P. G. Lagoudakis, A. V. Kavokin, J. J. Baumberg, G. Christmann, R. Butté, E. Feltin, J.-F. Carlin, and N. Grandjean, Phys. Rev. Lett. **98**, 126405 (2007).

[8] G. Christmann, R. Butté, E. Feltin, J.-F. Carlin, and N. Grandjean, Appl. Phys. Lett. **93**, 051102 (2008).

[9] H. Ajiki and H. Ishihara, J. Phys. Soc. Jpn. **76**, 053401 (2007).

[10] H. Oka, G. Oohata, and H. Ishihara, Appl. Phys. Lett. **94**, 111113 (2009).

[11] A. Tredicucci, Y. Chen, V. Pellegrini, M. Börger, L. Sorba, F. Beltram, and F. Bassani, Phys. Rev. Lett. **75**, 3906 (1995).

[12] A. Kavokin and B. Gil, Appl. Phys. Lett. **72**, 2880 (1998).

[13] G. Oohata, T. Nishioka, D. Kim, H. Ishihara, and M. Nakayama, Phys. Rev. B **78**, 233304 (2008).

[14] R. G. Ulbrich and C. Weisbuch, Phys. Rev. Lett. **38**, 865 (1977).

[15] A. V. Rodina, M. Dietrich, A. Göldner, L. Eckey, A. Hoffmann, Al. L. Efros, M. Rosen, and B. K. Meyer, Phys. Rev. B **64**, 115204 (2001).

[16] M. Ueta, H. Kanzaki, K. Kobayashi, Y. Toyozawa, and E. Hanamura, *Excitonic Processes in Solids* (Springer, New York, 1986), p. 116.

[17] P. Torchio, A. Gatto, M. Alvisi, G. Albrand, N. Kaiser, and C. Amra, Appl. Opt. **41**, 3256 (2002).

[18] K. Miyazaki, D. Kim, T. Kawase, M. Kameda, and M. Nakayama, Jpn. J. Appl. Phys. **49**, 042802 (2010).

[19] M. S. Skolnick, T. A. Fisher, and D. M. Whittaker, Semicond. Sci. Technol. **13**, 645 (1998).

[20] V. Savona, L. C. Andreani, P. Schwendimann, and A. Quattropani, Solid State Commun. **93**, 733 (1995).

[21] G. Panzarini, L. C. Andreani, A. Armitage, D. Baxter, M. S. Skolnick, V. N. Astratov, J. S. Roberts, A. V. Kavokin, M. R. Vladimirova, and M. A. Kaliteevski, Phys. Solid. Stat. **41**, 1223 (1999).

[22] W. Staude, Phys. Status Solidi B **43**, 367 (1971).

[23] F. Médard, J. Zuniga-Perez, P. Disseix, M. Mihailovic, J. Leymarie, A. Vasson, F. Semond, E. Frayssinet, J. C. Moreno, M. Leroux, S. Faure, and T. Guillet, Phys. Rev. B **79**, 125302 (2009).

[24] E. Mollwo, *Physics of II-VI and I-VII Compounds, Semimagnetic Semiconductors*, Landolt-Börnstein, New Series, Group III, Vol. 17b, edited by O. Madelung, M. Schulz, and H. Weiss (Springer, Berlin, 1982), p. 38.